

12-1996

Burst Pressure Prediction of Filament Wound Composite Pressure Vessels Using Acoustic Emission

Marcus Elwood Fisher

Embry-Riddle Aeronautical University - Daytona Beach

Follow this and additional works at: <https://commons.erau.edu/db-theses>



Part of the [Aerospace Engineering Commons](#)

Scholarly Commons Citation

Fisher, Marcus Elwood, "Burst Pressure Prediction of Filament Wound Composite Pressure Vessels Using Acoustic Emission" (1996). *Theses - Daytona Beach*. 289.

<https://commons.erau.edu/db-theses/289>

This thesis is brought to you for free and open access by Embry-Riddle Aeronautical University – Daytona Beach at ERAU Scholarly Commons. It has been accepted for inclusion in the Theses - Daytona Beach collection by an authorized administrator of ERAU Scholarly Commons. For more information, please contact commons@erau.edu.

**BURST PRESSURE PREDICTION OF FILAMENT WOUND COMPOSITE
PRESSURE VESSELS USING ACOUSTIC EMISSION**

by

Marcus Elwood Fisher

A Thesis Submitted to the Graduate Studies Office
in Partial Fulfillment of the Requirements for the Degree
of Master of Science in Aerospace Engineering

Embry-Riddle Aeronautical University

Daytona Beach, Florida

December 1996

UMI Number: EP31957

INFORMATION TO USERS

The quality of this reproduction is dependent upon the quality of the copy submitted. Broken or indistinct print, colored or poor quality illustrations and photographs, print bleed-through, substandard margins, and improper alignment can adversely affect reproduction.

In the unlikely event that the author did not send a complete manuscript and there are missing pages, these will be noted. Also, if unauthorized copyright material had to be removed, a note will indicate the deletion.

UMI[®]

UMI Microform EP31957
Copyright 2011 by ProQuest LLC
All rights reserved. This microform edition is protected against
unauthorized copying under Title 17, United States Code.

ProQuest LLC
789 East Eisenhower Parkway
P.O. Box 1346
Ann Arbor, MI 48106-1346

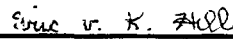
**BURST PRESSURE PREDICTION OF FILAMENT WOUND COMPOSITE
PRESSURE VESSELS USING ACOUSTIC EMISSION**

by


Marcus E. Fisher

This thesis was prepared under the direction of the candidate's thesis committee chairman, Dr. Eric v. K. Hill, Department of Aerospace Engineering, and has been approved by the members of his thesis committee. It was submitted to the School of Graduate Studies and Research and was accepted in partial fulfillment of the requirements for the degree of Master of Science in Aerospace Engineering.


THESIS COMMITTEE:



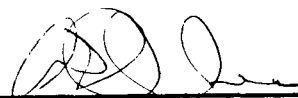
Dr. Eric v. K. Hill
Chairman



Dr. Frank Radosta
Member



Dr. Habib Eslami
Member



Department Chair, Aerospace Engineering

3/17/97

Date

ACKNOWLEDGMENTS

Writing this thesis has been the most grueling and enjoyable learning experience of my collegiate years. Though I was alone during the long hours I spent past midnight, I could not have done this without the help of a large number of allies.

First among them are my parents, Blanche and Elwood, their encouragement both morally and financially along with their sacrifices have given me this opportunity to further my education. I would also like to extend my thanks to my fiancée, Antonette, without her support and constant help this research would have never been completed.

I would like to acknowledge the seasoned professionals that have helped me in the preparation of this thesis. First for their service on my thesis committee, I would like to extend my sincere thanks to Dr. Frank Radosta and Dr. Habib Eslami for the work they have accomplished within the small time constraints to finish this research. I would also like to thank Dr. James Walker for his insight into neural networks and the testing of filament wound composite pressure vessels. Lastly, but certainly not least, a special thanks should go to Dr. Eric v. K. Hill. His faith in me along with the effort he has put into this research have made me extremely grateful that he showed interest in this student in his undergraduate composites class. He truly exemplifies what an advisor and friend should be.

ABSTRACT

Author: Marcus Elwood Fisher
Title: Burst Pressure Prediction of Filament Wound Composite Pressure Vessels Using Acoustic Emission
Institution: Embry-Riddle Aeronautical University
Degree: Master of Science in Aerospace Engineering
Year: 1996

This research demonstrates how acoustic emission (AE) data from flaw growth activity can be used to predict burst pressures in filament wound composite pressure vessels. Acoustic emission data were taken during hydroproof testing for a set of eleven ASTM standard 5.75 inch diameter fiberglass/epoxy bottles. Amplitude distributions were created using only the AE data up to 25% of the expected burst pressure to simulate low level proof loadings (thereby avoiding damage to the bottles). The bottles were tested at three different temperatures -- 32°F, 70°F, and 110°F -- and hydroproofed using two different pressurization schemes and two transducer configurations. Moreover, two of the bottles contained simulated manufacturing defects which lowered their burst pressures significantly.

Both multivariate statistical analysis and artificial neural networks were used to generate burst pressure prediction models from the AE amplitude distribution data. For the multivariate statistical analysis, fixed failure mechanism bands were applied to the amplitude distributions for all eleven fiberglass/epoxy bottles. The optimum failure mechanism bands resulted in a prediction equation that had a worst case prediction error of -14% and a correlation coefficient of 49.9%. When the defective bottles were left out of the analysis, the results improved to a +10% worst case error and a 65.0% correlation coefficient.

The amplitude distribution frequencies, temperatures, pressurization schemes, and transducer configurations were all used as inputs to the artificial neural networks. To begin with, the two pressurization schemes and the two transducer configuration schemes were found to have no significant effect on prediction accuracies. When one of the defective bottles was included in the training set and the other in the test set, the errors were +15.2% and +14.7%, depending upon which bottle was used for training and which for testing. Including both defective bottles in the training set decreased the worst case prediction error to -7.8%. Finally, when the two defective bottles were removed from consideration, the worst case prediction errors dropped to -0.8% and -1.5%, the former being obtained with temperature included as an independent variable and the latter without.

The neural networks predicted burst pressures to a greater accuracy than multivariate statistical analysis. This could be explained by the fact that the statistical analysis generates a linear burst pressure equation, whereas the neural network is not limited to linear modeling. The neural network results suggest that the addition of one defective bottle in the training set would probably allow the neural network to predict burst pressures with a worst case error within the desired goal of $\pm 5.0\%$. It can also be seen that, while the inclusion of temperature as one of the inputs to the neural network improves the prediction accuracy, the improvement does not appear to be significant.

TABLE OF CONTENTS

	Page
Signature Page	ii
Acknowledgments	iii
Abstract	iv
Table of Contents	vi
List of Tables	vii
List of Figures	viii
1.0 Introduction	1
2.0 Acoustic Emission	8
2.1 Event Parameters	8
2.2 AE Parameters of Failure Mechanisms	10
2.3 AE Amplitude Distribution	11
3.0 Statistical Analyses	14
3.1 Percentage of High Amplitude Events	14
3.2 Number of High Energy Events	16
3.3 Percentage of Failure Mode Types	17
4.0 Neural Networks	19
4.1 Algorithm and Example of Backpropagation Network	21
4.2 Prediction of Burst Pressures Using Neural Networks	24
5.0 Results	26
5.1 Statistical Analysis with Failure Mode Ranges	26
5.2 Neural Network Results	31
6.0 Conclusions and Recommendations	41
6.1 Conclusions	41
6.2 Recommendations	43
7.0 References	45
Appendix A Amplitude Distributions	48
Appendix B Sample MINITAB Regression Analysis	54

LIST OF TABLES

	Page
Table 2.1 Characterization of Fiberglass/Epoxy Failure Mechanisms Using AE Parameters	11
Table 5.1 Variables Used in the Multiple Regression Analysis	27
Table 5.2 Input Data for Statistical Analysis	28
Table 5.3 Failure Mechanism Ranges	29
Table 5.4 Input Data for Optimum Ranges for Statistical Analysis	30
Table 5.5 Neural Network Parameters	34
Table 5.6 Results of Neural Network using Temperature (1 Defect in Train; 1 Defect in Test)	35
Table 5.7 Results of Neural Network using Temperature (1 Defect in Train; 1 Defect in Test)	36
Table 5.8 Results of Neural Network using Temperature (Both Defective in Training Set)	37
Table 5.9 Results of Neural Network using Temperature (NO Defective Bottles)	38
Table 5.10 Results of Network With and Without Temperature (NO Defective Bottles)	39

LIST OF FIGURES

	Page
Figure 1.1 Percent Fiber Breaks vs. Percent Ultimate Load	1
Figure 1.2 Filament Wound Composite Pressure Vessel	3
Figure 1.3 Hydroproof Pressurization Schemes	4
Figure 1.4 Acoustic Emission Transducer Placement/Configurations	5
Figure 2.1 Resonant Piezoelectric Transducer	9
Figure 2.2 A Typical Acoustic Emission Signal and Parameters	9
Figure 2.3 AE Amplitude Distribution	12
Figure 3.1 Burst Pressure vs. Percentage of High Amplitude Events	15
Figure 3.2 Burst Pressure vs. High-Energy Events	16
Figure 3.3 Failure Mechanism Humps	18
Figure 4.1 Building Block of Neural Networks	19
Figure 4.2 Generic Neural Network Architecture	20
Figure 4.3 Simple Backpropagation Neural Network	22
Figure 5.1 Three Failure Mechanism Ranges within the AE Amplitude Distribution .	28
Figure 5.2 Neural Network for Burst Pressure Prediction	33

1.0 INTRODUCTION

Proof testing of composite structures is complicated by the fact that most composite structures do not exhibit the same elastic-plastic behavior found in metal structures. Excluding macroscopic flaws, as long as the stress is kept below the yield point, there is little plastic deformation and therefore no noticeable degradation in the structural integrity of metal structures. This does not hold true for fiber/matrix composites. Because the fibers are the primary load bearing constituents in composites, the structural integrity begins to degrade as soon as the fibers begin to break. For the fiber bundle shown in Figure 1.1, fiber breakage began to occur at less than 20 percent of the ultimate load [1]. While different structures might begin to experience fiber

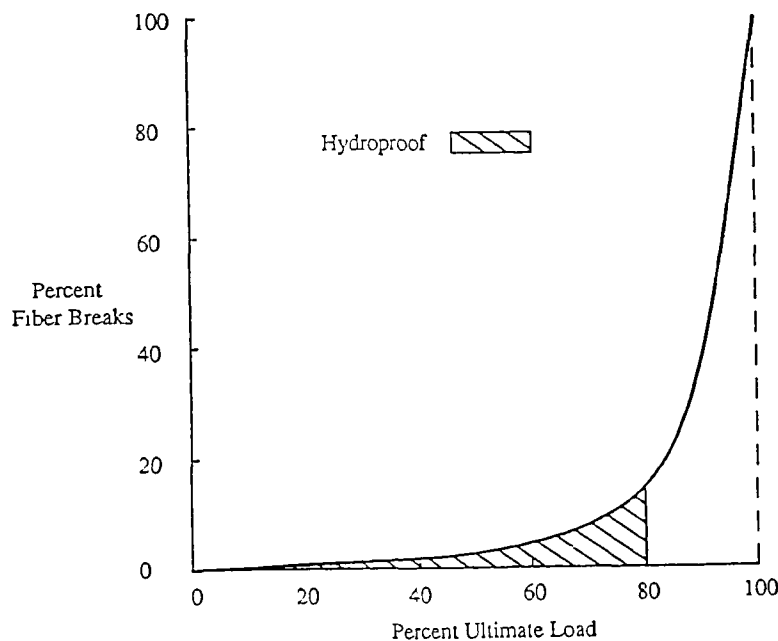


Figure 1.1 Percent Fiber Breaks vs. Percent Ultimate Load for a Fiber Bundle

breakage at a higher fraction of the ultimate load, the exponential upturn of the number of fiber breaks with increasing load is typical for composite structures. This means that the common proof testing loads of 70-80% of expected fracture strength used on metal designs can significantly damage a composite structure, thereby degrading its structural integrity. To avoid significant fiber breakage and the associated structural degradation during proof loading, a procedure needs to be adapted that uses a much lower proof loading for composites (25 percent of the ultimate load) and would, at the same time, accurately determine the ultimate strength of the structure.

The research performed herein utilized a series of eleven 5.75 inch diameter fiberglass/epoxy filament wound composite (FWC) pressure vessels also known as bottles. All the bottles employed S904 glass fibers and the ETC0021 resin type and were wet wound in a series of helical and hoop layers on a tumble winder at Morton Thiokol Inc. (Brigham City, UT) in 1984. Nine vessels were tested, three each at 30°F, 70°F, and 110°F, in order to ascertain the effect of temperature on the burst pressures. These vessels were used to simulate igniters for solid rocket motors, so these temperatures were significant in that 70°F is room temperature, 32°F is freezing, and 110°F is estimated to be the hottest that a rocket motor would get if the cooling system malfunctioned in a missile silo. The final two bottles had simulated manufacturing defects, where the outer hoop ply was shortened by 0.4 inches on one bottle and 0.6 inches on the other (Figure 1.2). Both of the defective bottles were tested at 70°F. Also, two different pressurization schemes were used to test the eleven bottles. The first one was a load-hold-unload type pattern as shown in Figure 1.3(a), and the second one was a simple ramp pressurization scheme shown in Figure 1.3(b). In terms of notation, the solid lines in Figures 1.3(a) and 1.3(b) indicate pressurization and acoustic emission (AE) data being considered simultaneously, whereas the broken lines indicate pressurization data only. Finally, two

different acoustic emission transducer configurations were used in monitoring the flaw growth activity during hydroproof. The locations of the transducers for each configuration are shown in Figure 1.4.

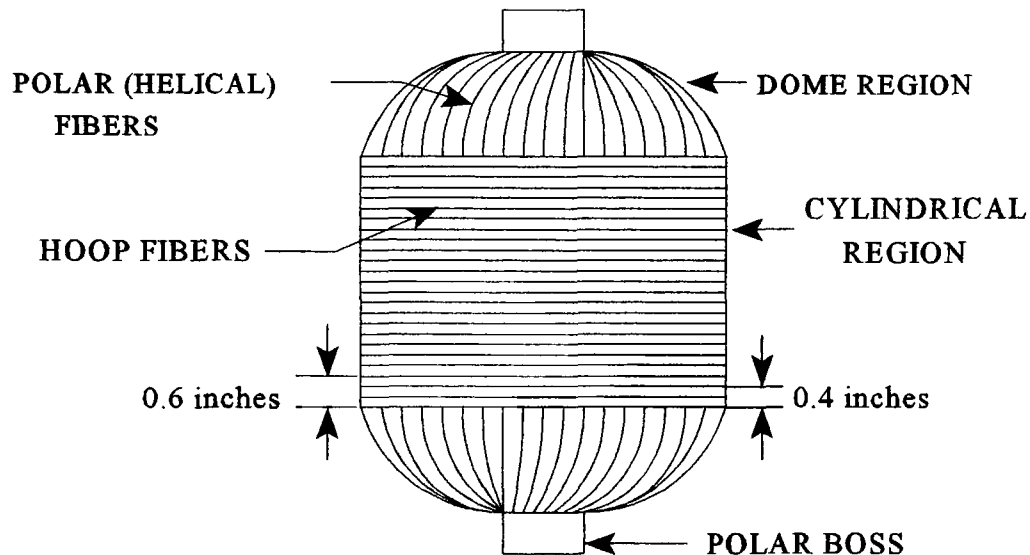
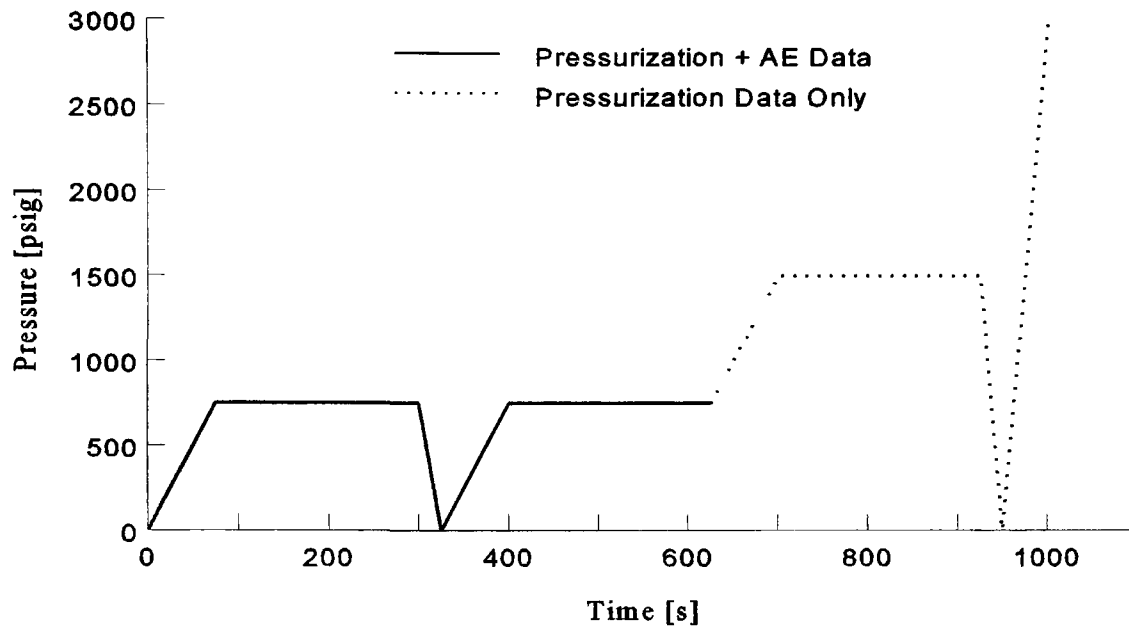
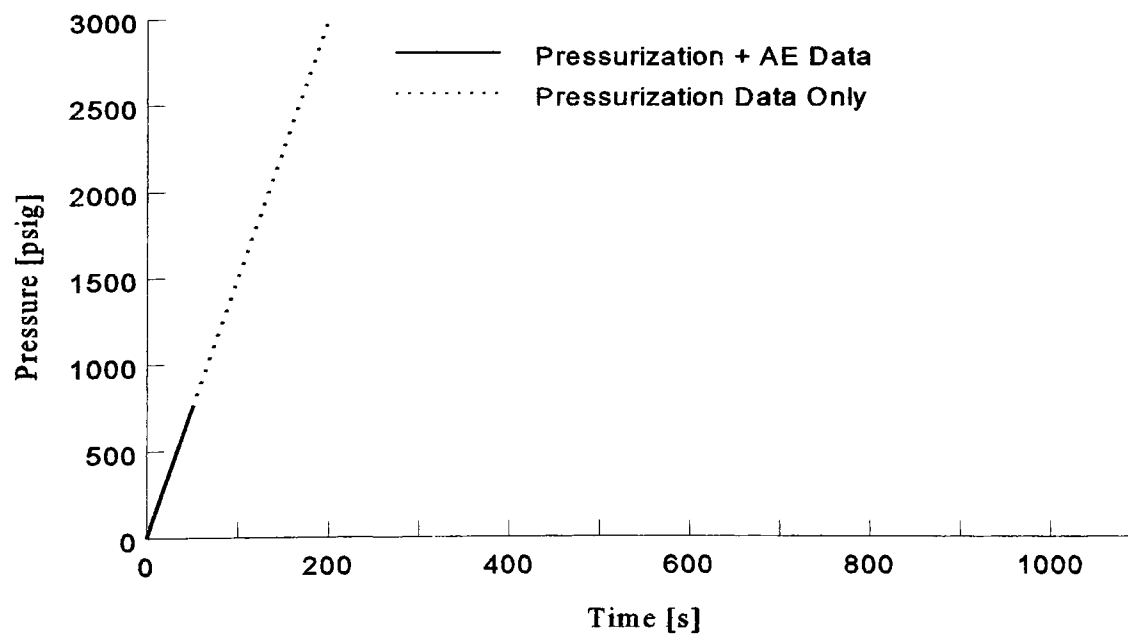


Figure 1.2 Filament Wound Composite Pressure Vessel

The manufacturing process of FWC pressure vessels begins with the filament winding process. This process starts with a fiber such as Kevlar, graphite, or for this research fiberglass passing through a liquid bath of resin and then being wound around a rubber coated, compressed sand mandrel in a series of helical and hoop layers as shown in Figure 1.1. The structure is then cured in an oven, and finally the sand mandrel is washed from the inside of the bottle using a water jet. The composite pressure vessel thus formed has a high strength to weight ratio; hence, FWC pressure vessels have replaced metal pressure vessels in many aerospace applications such as rocket motor cases.



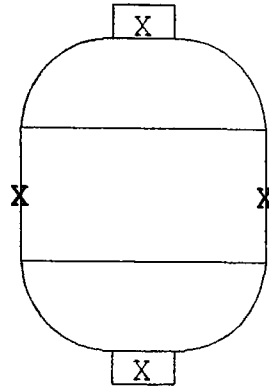
(a) Load-Hold-Unload Pressurization Scheme



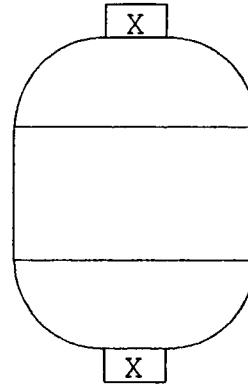
(b) Simple Ramp Pressurization Scheme

Figure 1.3 Hydroproof Pressurization Schemes

Transducer Configuration 1



Transducer Configuration 2



X - Transducer Location

Figure 1.4 Acoustic Emission Transducer Placement/Configurations

Filament wound composite pressure vessels have three primary failure mechanisms: matrix cracking, delaminations, and fiber breaks. The purposes of the matrix are to protect the fibers, hold the fibers in place, and to transmit the loads to the fibers. Because the fibers are the primary load bearing constituents of the structure, fiber breaks are the most critical failure mechanism in determining the burst strength. However, during a normal hydroproof test, a significant number of fiber breaks can occur, which will drastically lower the burst pressure of the bottle. Matrix cracking and delaminations can also occur during hydroproof, changing the expected burst pressure of the vessels, but to a lesser extent than fiber breaks.

Acoustic emission technology has proven to be very useful in classifying these failure mechanisms, in that each of the mechanisms possesses a different acoustic emission signature (Section 2.1). These acoustic signatures will be used to determine the effect of the various failure mechanisms on the burst pressure. Acoustic emission nondestructive testing is utilized primarily for its ability to monitor structures in real time

on a global basis. Acoustic emission is produced by the rapid release of strain energy as microscopic and macroscopic flaw growth occurs in a structure. The stress waves produced by this release of energy travel radially outward from the flaw growth sources. Piezoelectric transducers are placed on the bottle to convert these stress waves into electric voltage signals which are then used for analysis (Section 2.0).

The amount of acoustic emission activity provides a quantitative measure of structural integrity. Stress concentrations in the composite structure such as misaligned fibers, resin starved areas, etc., can greatly reduce the overall strength of the structure. Such stress concentrations are typically very acoustically active from the onset of pressurization. As such, acoustic emission has been used to determine the overall strength of structures at low proof loads.

It was demonstrated by Kalloo [2] that AE data and multivariate statistical analysis could be used to predict burst pressures in graphite/epoxy pressure vessels. Then Walker [3] showed that AE data could be used along with multivariate statistical analysis in determining equations for ultimate strength prediction in ASTM D-3039 unidirectional graphite/epoxy tensile specimens. Subsequently, Walker and Hill [4] solved this problem using neural networks; and then Hill, Walker, and Rowell [1] applied neural networks to generate a burst pressure prediction model on a series of 5.75 inch diameter graphite/epoxy bottles (using three different resin types).

The research presented herein uses the multivariate statistical analysis and neural network techniques to predict burst pressures in a series of eleven fiberglass/epoxy pressure vessels. The bottles used for this research are different from previous research in the fact that the three temperatures, the two pressurization schemes, and the two transducer configurations were all used while hydroproofing the bottles. Also, the fact that manufactured defective bottles are used is different than what Hill, Walker, and

Rowell have done with neural networks. AE data were collected during the hydroproof cycle; however, only the data up to 25% of the expected burst pressure were used for the analysis herein to simulate proof loadings of 25% of fracture strength. Both multivariate statistical analysis and artificial neural networks will be applied to the AE data from the eleven bottles to generate burst pressure prediction models. It will be determined if either or both methods can accurately predict burst pressures in the vessels including the two bottles with simulated manufacturing defects (premature hoop fiber reversals).

2.0 ACOUSTIC EMISSION

To understand how acoustic emission nondestructive testing can be used to predict burst pressures in FWC pressure vessels, some background knowledge of acoustic emission must be provided. An AE signal is produced by the rapid release of strain energy as flaw growth occurs in a material. Energy waves (or stress wave packets) are produced from this release of energy and travel outward from the flaw growth source. The stress waves either couple into the water or mode convert and propagate along the boundaries of the structure as surface waves.

Piezoelectric transducers are placed on the bottle to convert the stress waves into electric voltage signals which are then used for analysis. Resonant (narrow band) transducers (Figure 2.1) are used in this application because of their ability to pick up low amplitude signals. Pre-amplifiers are placed in the circuit near the transducer and shielded cables are used to eliminate interference. The pre-amplifier is usually set to a 40 dB gain which magnifies the signal by a factor of 100. Bandpass filters are also used to block out low and high frequencies such as hydraulic or mechanical noises and electromagnetic interference.

2.1 EVENT PARAMETERS

A typical acoustic emission signal (Figure 2.2) is a complex, damped, sinusoidal voltage versus time trace. As shown, some of the parameters used to quantify acoustic

emission signals are events, counts, amplitude, duration, and energy. The adjustable threshold voltage is set above the noise level of the signal such that no signals will be recorded below this voltage.

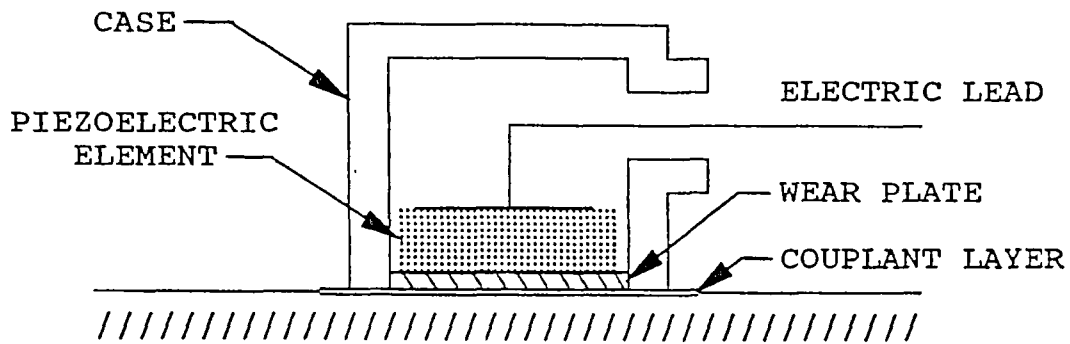


Figure 2.1 Resonant Piezoelectric Transducer [3]

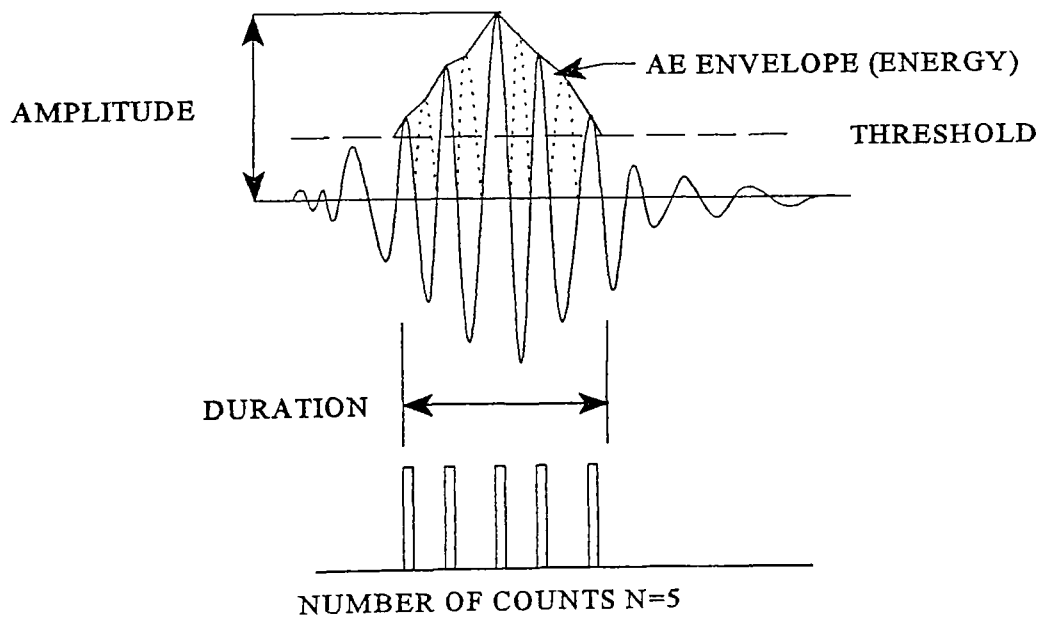


Figure 2.2 A Typical Acoustic Emission Signal and Parameters

An event begins when the signal voltage first surpasses the threshold and ends when the signal goes below the threshold for a specified period of time (say 200 μ s). The counts parameter is the number of times the signal amplitude exceeds the threshold during the event. The total time the event lasts is known as duration and is measured in microseconds. Energy is the area under the rectified and squared event envelope. The peak amplitude, or simply the amplitude, is the maximum voltage the signal attains for a given event. Since AE amplitudes typically range from a few microvolts up to tens of volts, in order to get them all on one plot, the amplitude parameter is measured and plotted on a logarithmic scale (see Section 2.3).

2.2 AE PARAMETERS OF FAILURE MECHANISMS

As was mentioned previously, the three primary failure modes for most composites are matrix cracking, fiber breakage, and delaminations. Each of these failure modes has characteristic magnitudes for the various AE parameters, which makes acoustic emission useful in identifying these failure mechanisms.

Matrix cracking occurs throughout the testing cycle and is usually the least damaging of the mechanisms. A typical matrix crack signal is of short duration with a small amplitude and low energy. Delaminations occur when the laminae begin to shear apart. This mechanism can increase the burst pressure by reducing the interlaminar shear stresses within a vessel [5]. A delamination signal can be visualized as a series of overlapping matrix crack signals; therefore, the duration will be much longer, the energy will be greater, and the amplitude will be higher than those of a single matrix cracking signal. The last failure mode, fiber breakage, is typically the most damaging of the mechanisms, since the fibers are the main load bearing constituents of the structure.

Glass fiber breaks have very short durations and the highest amplitudes of the three primary failure mechanisms. The failure mechanisms with their typical acoustic emission values are summarized in Table 2.1. Although all the parameters are useful in providing information on acoustic emission, the research herein will only use the amplitude parameter (in the form of amplitude distribution plots) for burst pressure prediction.

Table 2.1 Characterization of Fiberglass/Epoxy Failure Mechanisms Using AE Parameters

AE Parameters	Failure Mechanisms		
	Matrix Cracking	Delaminations	Fiber Breaks
Counts	Low	High	Low-Medium
Amplitude	Low	High	Very High
Energy	Low	High	Medium-High
Duration	Short	Long	Short-Medium

2.3 AE AMPLITUDE DISTRIBUTION

The AE amplitude data can be graphed into an amplitude vs. events histogram known as an amplitude distribution plot (Figure 2.3). Peak signal voltages of the AE signals range from 0 dB (100 μ V) to 100 dB (10 V), where amplitude A [dB] is a logarithmic representation of the peak signal voltage, V [V], of the AE waveform:

$$A = 20 \log (V / V_{\text{ref}}).$$

Typically, $V_{\text{ref}} = 1 \mu\text{V}$ at the sensor output is chosen as the 0 dB reference because it is slightly above the noise level of the system electronics.

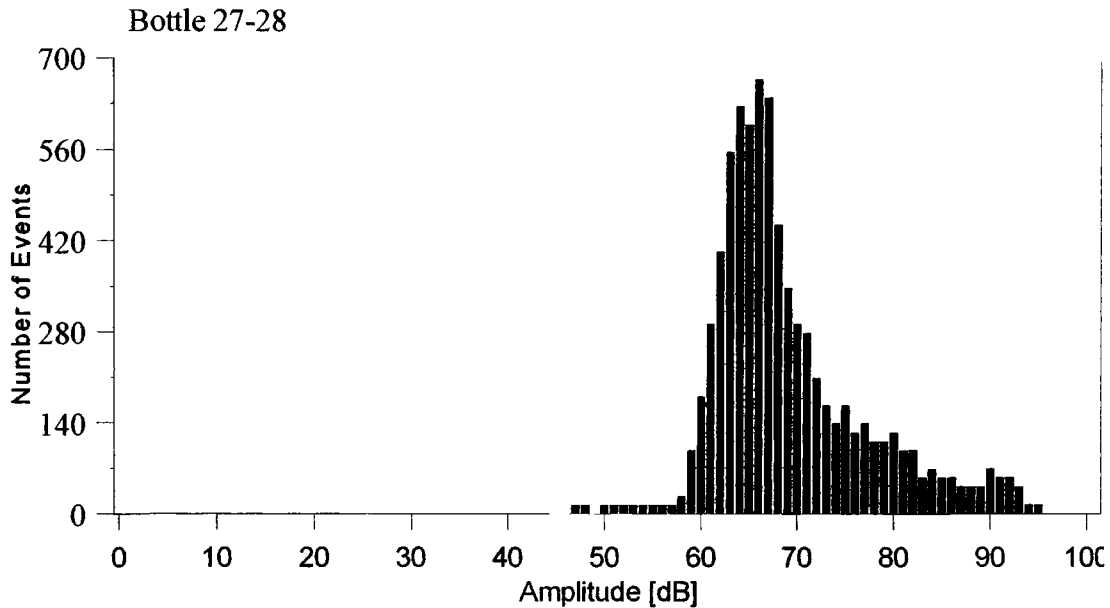


Figure 2.3 AE Amplitude Distribution

Previous experiments have shown that the failure mechanisms are grouped together in characteristic overlapping humps in the amplitude distribution. Since the logarithms of measurements tend to have normal distributions [6,7], the humps were approximated as such. Kalloo [2] modeled these humps and determined their effects on the structural integrity of graphite/epoxy pressure vessels, using multivariate statistical analysis to generate a burst pressure prediction equation.

In 1994 Hubele and Hwarng [8] showed that a three layer backpropagation neural network could closely approximate the results obtained from statistical analysis. Neural network approximations also take into account any nonlinearities present, and according to the Kolmogorov theorem, a three layer neural network should be able to map any

continuous function exactly [9]. Therefore, since statistics are capable of predicting burst pressures in composite pressure vessels, neural networks should be capable of doing the same thing.

Because of extensive overlap in the amplitude distribution data, an exact determination of the failure mechanism humps is not possible. A procedure needs to be implemented that will automatically determine the failure mechanism bands and thereby eliminate human error. The first technique to be used for this research involves setting a fixed decibel range for each of the three humps, and then applying these ranges to all eleven sets of bottle data. The second technique uses the event frequencies for each 1 dB amplitude interval (instead of the mechanism frequencies associated with each of the three humps) as inputs to a neural network. This will provide a more detailed picture from which to derive the predictions.

3.0 STATISTICAL ANALYSES

Multivariate statistical analysis has been used with the AE amplitude data to determine burst pressure equations. The percentage of high amplitude AE events, the number of high energy events, and the percentage of the total events in each failure mechanism hump have all been used to accurately predict burst pressures. These techniques are summarized below.

3.1 PERCENTAGE OF HIGH AMPLITUDE EVENTS

Delaminations and fiber breaks have been determined to be the most damaging of the three primary failure mechanisms experienced with composite pressure vessels. Through previous experimentation, it has been determined that AE amplitudes above 70 dB were produced by these two mechanisms. Therefore, a measure of the integrity of the vessel is provided by the high amplitude AE data.

Hill [10] has shown that a burst pressure prediction equation could be generated by using the percentage of high amplitude AE events for a series of six 18 inch diameter graphite/epoxy pressure vessels. Using AE data recorded up to 12.5% of the expected burst pressure, a prediction equation was generated to within $\pm 3.0\%$ worst case error with a 95% prediction interval.

Using a stepwise linear analysis of the data with several candidate variables, Hill found that only the percentage of high amplitude events and the prepreg batch

contributed significantly to the model. The burst pressure equation thus became

$$\begin{aligned} \text{BRSTPRS} = & -378.8 + 4539 \text{ PCTHAE} + 3053 \text{ PREPREG} \\ & - 3600 \text{ PCTHAE} * \text{PREPREG}, \end{aligned}$$

where

BRSTPRS = Burst Pressure (psig)

PCTHAE = Percentage of high amplitude events

PREPREG = Prepreg batch (0, 1, -1 depending upon batch number).

The cross-product term PCTHAE*PREPREG was needed to account for the interaction between the AE amplitudes and the prepreg batch. This can be seen in the crossed lines of Figure 3.1. Physically the two resins will have differences in their stiffness, therefore, the two resins will have different acoustic attenuation properties. Thus, two distinctly different amplitude distributions were produced by the two resin batches.

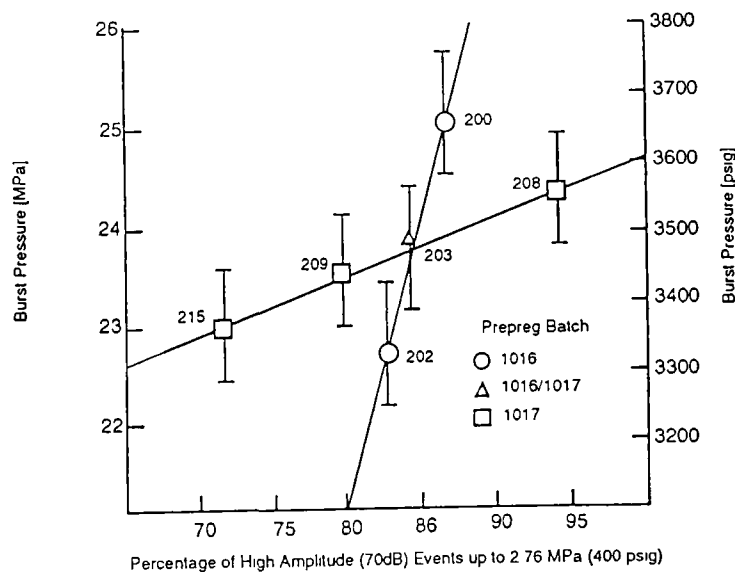


Figure 3.1 Burst Pressure vs. Percentage of High Amplitude Events [10]

3.2 NUMBER OF HIGH ENERGY EVENTS

Hill [10] employed a similar technique on the fiberglass/epoxy bottles (analyzed herein) to generate a prediction equation for burst pressures. He used the number of high energy events (≥ 500 units) as the primary independent variable in the prediction equation. Plotting burst pressure vs. high energy AE events (Figure 3.2) yields two parallel lines representing the two pressurization schemes used to test these bottles. Bottle 78-112 was thought to be an outlier and was not included in generating the prediction equation. The burst pressure equation was thus determined to be

$$\text{BRSTPRS} = 2093 + 46.20 \text{ HEEVNTS} - 506.1 \text{ PRSSCHM (psig)}.$$

This equation predicted burst pressures to an accuracy of ± 4.35 percent.

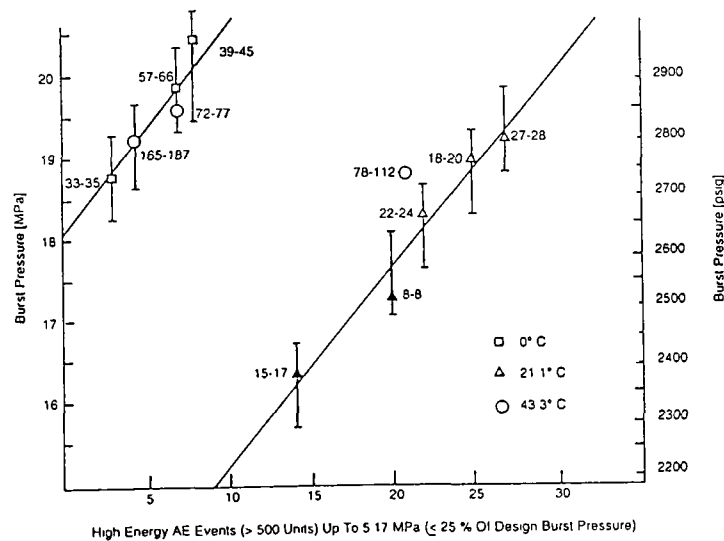


Figure 3.2 Burst Pressure vs. High-Energy Events [10]

3.3 PERCENTAGE OF FAILURE MODE TYPES

Kaloo [2] used the percentage of amplitude based failure mechanisms to determine burst pressures in a series of ASTM 5.75 inch diameter graphite/epoxy pressure vessels. Using Rayleigh and Gaussian distributions to model the three failure mechanism humps, Kaloo demonstrated that multivariate statistical analysis could be used to form a linear equation for burst pressure (P_b) prediction of the following form:

$$P_b = \beta_0 + \beta_1 M_1 + \beta_2 M_2 + \beta_3 M_3 .$$

Here β_0 is the coefficient for the unflawed pressure vessel strength; β_1 , β_2 , β_3 are the coefficients associated with matrix cracking, fiber breaks, and delaminations, respectively; and M_1 , M_2 , M_3 are the event fractions contained within each failure mechanism hump. Determining the amplitude ranges of these humps by hand, Kaloo generated an equation that predicted burst pressures to within $\pm 1.0\%$ of the expected value. Here the AE data up to 25% of the expected burst pressure were used for the eleven bottles tested.

Kaloo determined through experimentation that the first hump in the amplitude distribution, which corresponds to the matrix cracking failure mechanism, was best modeled as a Rayleigh type curve. The two remaining humps were represented as Gaussian distributions. This can be seen in Figure 3.3.

Kaloo modeled the three humps for each failure mechanism, and then determined the percentage of events under each curve. The event percentages for each hump were then used to generate the burst pressure prediction equation

$$P_b = 4563.3 - 1433.6 V1 - 3661.8 V2 + 2864.9 V3 \quad (\text{psig}),$$

where V1 is the percentage of failure mechanisms under the first Rayleigh hump, and V2 and V3 are the percentage of events under the two Gaussian humps.

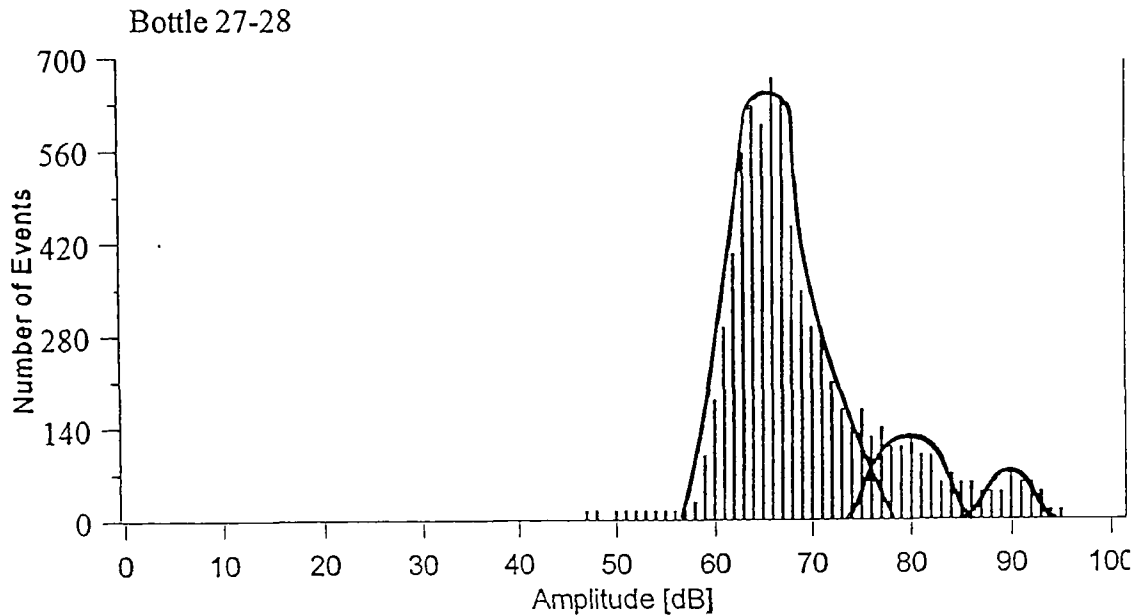


Figure 3.3 Failure Mechanism Humps

Kaloo demonstrated that burst pressures could be predicted accurately using this technique, but the repeatability of his technique is uncertain. Determining the Rayleigh and Gaussian distributions by hand for each amplitude distribution, as he did, would be difficult to duplicate let alone automate. The results could vary significantly due to slight differences in the modeling of the three failure mechanism humps. An automated version of this technique will be employed here in an attempt to predict burst pressures for the eleven fiberglass/epoxy bottles being analyzed for this research.

4.0 NEURAL NETWORKS

An artificial neural network is an information processing system that has certain characteristics similar to biological neural networks. A neural network consists of a large number of simple processing elements called neurons or nodes (Figure 4.1). Each of these neurons is connected to other neurons by communication links, each with an associated weight. The weights represent information being used by the network to solve a problem. A neuron has many input paths and combines the values of the input paths by a simple summation. The summed input is then modified by a transfer function and passed directly to the output path of the processing element.

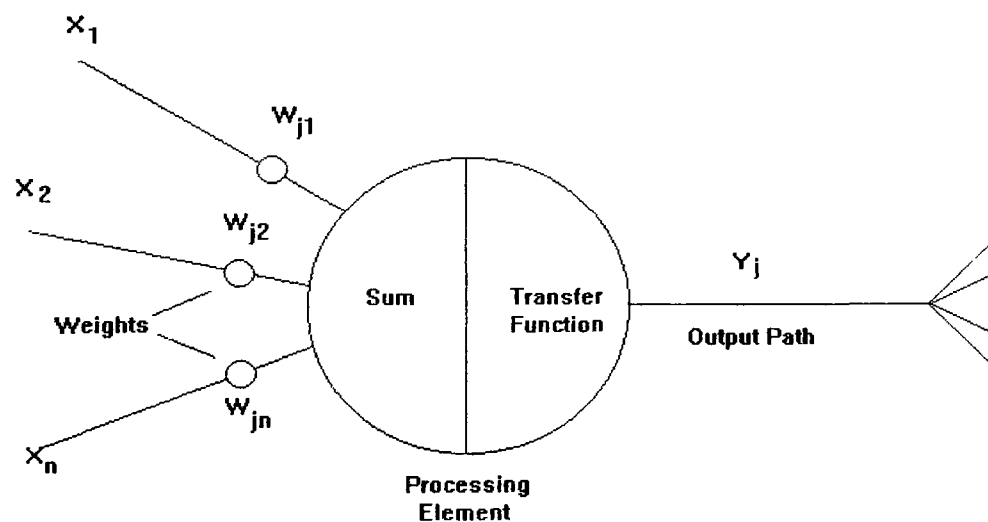


Figure 4.1 Building Block of Neural Networks

The output path of the processing elements can then be connected to input paths of other nodes through connection weights. Since each connection has a corresponding weight, the signals on the input lines to a processing element are modified by these weights prior to being summed. The processing elements are usually organized into groups called layers. Typically a network consists of an input layer, where data is presented to the network, and output layer which holds the response of the network, and one or more hidden layers for processing as shown in Figure 4.2.

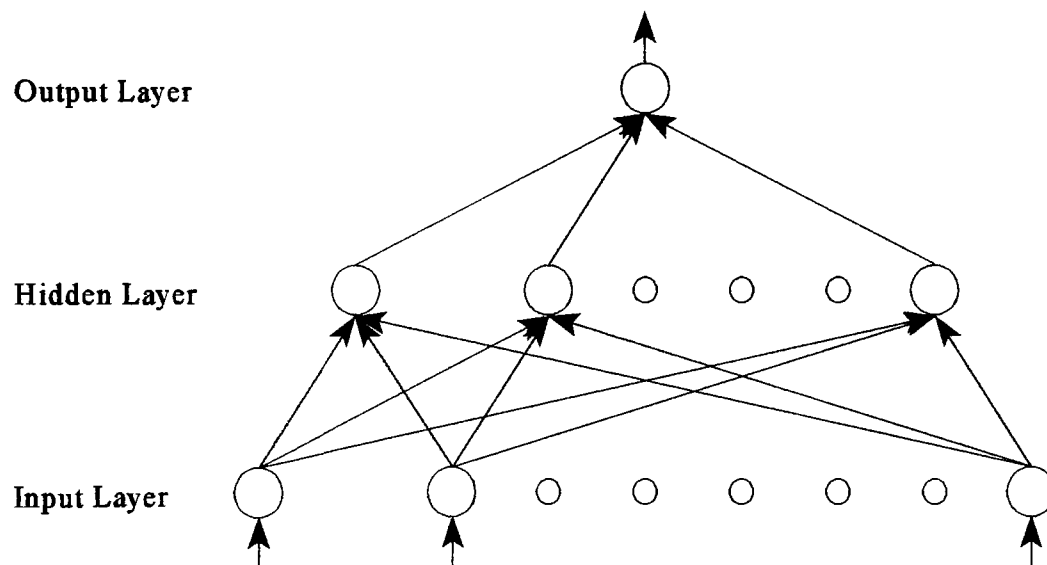


Figure 4.2 Generic Neural Network Architecture

There are several types of neural networks, but only feedforward backpropagation networks will be discussed here. A feedforward network is one that has no feedback connections from one layer to another or to itself. Information is passed from the input buffer through the hidden layers to the output layer in a straightforward manner using the summation and transfer function characteristics of the network.

There are two main phases in the operation of a feedforward backpropagation neural network, learning and recall. Learning is the process the network goes through to adapt or modify the connection weights. The type of learning used in this type of network is called “supervised learning.” This is when the desired response or output of the network is given; in this case, the network is given the actual burst pressure for each of the bottles used in the learning phase. Recall refers to how the network processes a stimulus presented at its input layer and creates a response at the output layer. Recall is part of the learning process where the desired response of the network is compared to the actual output of the network to create an error signal. The error signal is then used to modify the connection weights throughout the network or “back propagate” the error. This technique is demonstrated in the example that follows.

4.1 ALGORITHM AND EXAMPLE OF BACKPROPAGATION NETWORK

The training of a backpropagation network involves three stages: (1) the feedforward of the input training pattern, (2) the backpropagation of the associated error, and (3) the adjustment of the connection weights. Following is the algorithm for a sample backpropagation neural network.

First Stage: Forward Propagation Through Network

Step 0. Initialization of weights (small random values between 0.0 and 1.0

or -1.0 and 1.0, depending upon the activation function.)

Step 1. While stopping condition is false, do steps 2-8

Step 2. Compute input sum and apply activation function for each hidden layer neuron

Step 3. Compute input sum and apply activation function for each output layer neuron

Second Stage: Backpropagation of Error

- Step 4. Compute network error
- Step 5. Compute delta weights
- Step 6. Compute error contribution for each middle layer neuron
- Step 7. Compute delta weights for middle layer

Third Stage: Adjustment of Connection Weights

- Step 8. Update weights
- Step 9. Test stopping condition

EXAMPLE: A simple backpropagation neural network with 2 inputs, a single hidden layer with 2 neurons, and a single output (Figure 4.3).

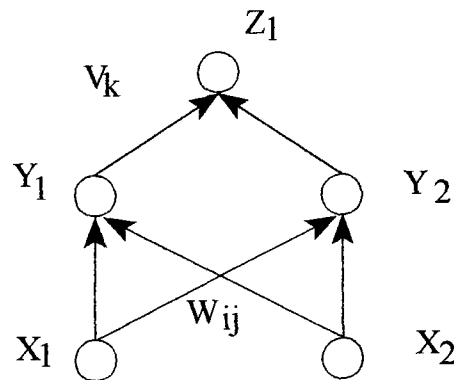


Figure 4.3 Simple backpropagation neural network

The input vector is $X_i = [1.0, 0.0]$, and the target output vector is $T_1 = 1.0$. Use a learning coefficient $LC = 0.25$ and a sigmoid activation function (random initial weights between -1.0 and 1.0).

First Stage: Forward Propagation Through Network

Step 0: Initialization of weights

$$W_{ij} = 0.8 \ 0.5 \ ; \ -0.6 \ 0.3$$

$$V_k = 0.7 \ 0.2$$

Step 1: While stopping condition is false

Step 2: Compute input sum and apply activation function for each hidden layer neuron

$$y_1 = (W_{11})(X_1) + (W_{21})(X_2) = (0.8)(1.0) + (-0.6)(0.0) = 0.8$$

$$y_2 = (W_{12})(X_1) + (W_{22})(X_2) = (0.5)(1.0) + (0.3)(0.0) = 0.5$$

$$Y_{1(out)} = f(y_1) = 1/(1 + e^{-y_1}) = 0.69$$

$$Y_{2(out)} = f(y_2) = 1/(1 + e^{-y_2}) = 0.62$$

Step 3. Compute input sum and apply activation function for each output layer neuron

$$z_1 = (V_{11})(Y_1) + (V_{12})(Y_2) = (0.7)(0.69) + (0.2)(0.62) = 0.61$$

$$Z_{1(out)} = f(z_1) = 0.65$$

Second Stage: Backpropagation of Error

Step 4. Compute network error

$$\delta_k = \delta_{z1} = (T_1 - Z_1) * f(z_1) * (1 - f(z_1)) = (1.0 - 0.65) * (0.65) * (1 - 0.65) = .080$$

Step 5. Compute delta weights

$$\Delta V_{jk} = \Delta V_{11} = LC * \delta_{z1} * Y_1 = 0.25 * 0.080 * 0.69 = 0.014$$

$$\Delta V_{jk} = \Delta V_{12} = LC * \delta_{z1} * Y_2 = 0.25 * 0.080 * 0.62 = 0.012$$

$$V_{11(new)} = 0.7 + 0.014 = 0.714$$

$$V_{12(new)} = 0.2 + 0.012 = 0.212$$

Step 6. Compute error contribution for each middle layer neuron

$$\delta_{y1} = \delta_{z1} * V_{11} * f(y_1) * (1 - f(y_1))$$

$$= 0.080 * 0.7 * 0.69 * (1 - 0.69) = 0.012$$

$$\delta_{y2} = \delta_{z1} * V_{21} * f(y_2) * (1 - f(y_2))$$

$$= 0.080 * 0.2 * 0.62 * (1 - 0.62) = 0.0038$$

Step 7. Compute delta weights for middle layer

$$\Delta W_{11} = LC * \delta_{Y1} * X_1 = 0.25 * 0.012 * 1.0 = 0.003$$

$$\Delta W_{12} = LC * \delta_{Y1} * X_2 = 0.25 * 0.012 * 0.0 = 0.0$$

$$\Delta W_{21} = LC * \delta_{Y2} * X_1 = 0.25 * 0.0038 * 1.0 = 0.00095$$

$$\Delta W_{22} = LC * \delta_{Y2} * X_2 = 0.25 * 0.0038 * 0.0 = 0.0$$

$$W_{11(\text{new})} = 0.8003$$

$$W_{12(\text{new})} = 0.5$$

$$W_{21(\text{new})} = -0.599$$

$$W_{22(\text{new})} = 0.3$$

Second Pass Output = 0.652

4.2 PREDICTION OF BURST PRESSURES USING NEURAL NETWORKS

Hill, Walker, and Rowell [1] used an artificial neural network to predict burst pressures in a series of seventeen 5.75 inch diameter filament wound graphite/epoxy bottles. The network predicted burst pressures in this set of bottles with a worst case error of - 3.89%. The neural network architecture used for this application consisted of a forty-eight neuron input layer, a fifteen neuron hidden layer, and a single output neuron for burst pressure prediction. Nine of the bottles were used to train the network, while the remaining eight bottles were used to “blind” test the network. Blind testing is used to determine the burst pressure prediction accuracy of the network for bottles on which it has not been trained.

A categorical variable for resin type was generated for each of the three sets of

bottles. This categorical variable was used as an input for the neural network. This allowed the network to easily recognize the different resin types. The categorical variable along with the forty-seven integer variables for the AE amplitude distribution frequencies were used as inputs to the forty-eight neuron input layer.

5.0 RESULTS

Multivariate statistical analysis and artificial neural networks were used herein to predict burst pressures (within a desired goal of $\pm 5\%$ error) for eleven 5.75 inch diameter filament wound fiberglass/epoxy pressure vessels. Both analyses employed the acoustic emission amplitude parameter with the data taken up to 25% of the expected burst pressure.

One source of possible error came from the resolution of the amplitude distributions. For example, the data for bottle 72-77 plotted the event frequencies in multiples of three, whereas bottle 15-17 plotted the event frequencies in multiples of twenty-one (Appendix A). This significant difference in scale could cause errors in the prediction routines.

5.1 STATISTICAL ANALYSIS WITH FAILURE MODE RANGES

The procedure used for this part of the research is similar to that of Kalloo's thesis (section 3.2), where the amplitude distribution was broken up into three failure mechanism modes: fiber breaks, delaminations, and matrix cracks. As stated previously, the bottles were tested using two different pressurization schemes, at three different temperatures, and with two different transducer configurations. These three variables were used in the regression analysis as shown in Table 5.1.

Table 5.1 Variables Used in the Multiple Regression Analysis

Dependent Variable	Numerical Values
Burst Pressure (BrstPress)	---
Independent Variables	
1. Percentage of Matrix Cracks Failure Mode (FM1)	---
2. Percentage of Delaminations Failure Mode (FM2)	---
3. Percentage of Fiber Breaks Failure Mode (FM3)	---
4. Burst Temperature (Temp)	
a. 32°F	32
b. 70°F	70
c. 110°F	110
5. Pressurization Scheme (PressSch)	
a. load-hold-unload	1
b. ramp to failure	0
6. Transducer Configuration (Trans)	
a. transducers 1&4 on polar bosses transducers 2&3 on cylinder	1
b. transducers 1&3 on polar bosses	0

Kaloo modeled the amplitude distributions using Raleigh and Gaussian distributions for the failure mechanism humps and then used the percentage of total events under each as inputs for the statistical analysis. Here in order to keep human error and judgement out of the testing procedure, it was decided to use specific amplitude bands as the cutoff points for each failure mechanism. The cutoff points for matrix cracking were approximated to be between 60-79 dB, with delaminations between 80-88 dB, and fiber breaks between 89-100 dB (Figure 5.1). These same amplitude ranges were used for all eleven pressure vessels. The numbers of events for each range were then counted and converted into failure mechanism percentages by dividing by the total

number of events occurring for each bottle. The percentages of events for each failure mechanism were then tabulated (Table 5.2) and entered into the Student Edition of the MINITAB software package.

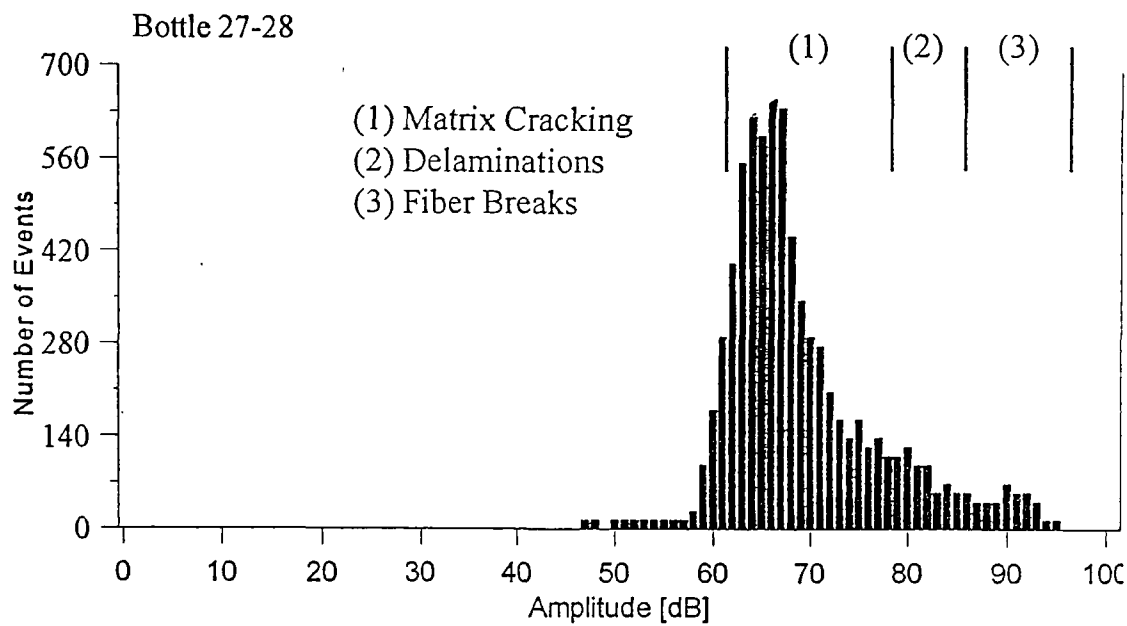


Figure 5.1 Three Failure Mechanism Ranges within the AE Amplitude Distribution

Table 5.2 Input Data for Statistical Analysis

Bottle Number	Burst Pressure (psi)	Failure Mode 1	Failure Mode 2	Failure Mode 3	Burst Temp.(°F)	Pressure Scheme	Transducer Location
15-17	2257	0.925	0.056	0.019	70	1	1
8-8	2444	0.908	0.065	0.026	70	1	1
22-24	2636	0.934	0.044	0.022	70	1	1
18-20	2773	0.938	0.042	0.021	70	1	1
27-28	2816	0.875	0.086	0.039	70	1	0
33-35	2730	0.941	0.041	0.018	32	0	0
78-112	2754	0.958	0.033	0.009	110	0	0
165-187	2789	0.959	0.031	0.009	110	0	0
72-77	2833	0.962	0.036	0.002	110	0	0
57-66	2887	0.960	0.030	0.011	32	0	0
39-45	2959	0.969	0.027	0.004	32	0	0

A multiple regression analysis was performed to obtain an equation for burst pressure prediction using the subroutine REGRESS (Appendix B). The equation generated was in the same basic form as that used by Kalloo, a linear equation for burst pressure (Section 3.2). The equation generated using this procedure yielded unacceptably large errors (near 25%). Along with high percent errors, the multiple correlation coefficient was only 45.9%. This meant that only 45.9 percent of the variability in the data was accounted for by the prediction equation.

The 25% error using the initial failure mode limits was considered to be unacceptably large. Therefore, it was decided to perform several iterations with various failure mechanism ranges in order to optimize the procedure. The various limits used along with the largest percent error and the multiple correlation coefficient values are presented in Table 5.3.

Table 5.3 Failure Mechanism Ranges

Matrix Cracking Range (dB)	Delamination Range (dB)	Fiber Break Range (dB)	Largest Percent Error	Multiple Correlation Coef
60-79	80-88	89-100	25 %	45.9 %
60-77	78-88	89-100	+ 28 %	40.3 %
60-81	82-90	91-100	- 33 %	35.8 %
60-76	77-89	90-100	- 18 %	58.6 %
60-80	81-88	89-100	+ 21 %	50.2 %
60-75	76-86	87-100	- 14 %	65.0 %

Changing the matrix cracking limit to 60-75 dB, delaminations to 76-86 dB, and fiber breaks to 87-100 dB was found to be optimum for the ranges tested. This resulted in the failure mechanism percentages listed in Table 5.4.

Table 5.4 Input Data for Optimum Ranges for Statistical Analysis

Bottle Number	Burst Pressure (psi)	Failure Mode 1	Failure Mode 2	Failure Mode 3	Burst Temp.(°F)	Pressure Scheme	Transducer Location
15-17 Def.	2257	0.870	0.102	0.028	70	1	1
8-8 Def.	2444	0.857	0.106	0.037	70	1	1
22-24	2636	0.890	0.079	0.031	70	1	1
18-20	2773	0.889	0.083	0.028	70	1	1
27-28	2816	0.809	0.140	0.051	70	1	0
33-35	2730	0.909	0.068	0.023	32	0	0
78-112	2754	0.911	0.075	0.014	110	0	0
165-187	2789	0.922	0.063	0.015	110	0	0
72-77	2833	0.927	0.066	0.007	110	0	0
57-66	2887	0.909	0.078	0.013	32	0	0
39-45	2959	0.921	0.073	0.006	32	0	0

The equation generated using the last set of failure mode ranges yielded better results than the previous ranges. The accuracy of the burst pressure equation improved from 25% down to -14%, while the multiple correlation coefficient increased from 45.9% to 65%, meaning that 65% of the variability in the data was accounted for by the prediction equation. Note that the regression analysis used only the first failure mode (matrix cracking) to generate the equation

$$\text{BrstPress} = -6066 + 9836 \text{ FM1} - 1.74 \text{ Temp} + 1046 \text{ PresSch} - 952 \text{ Trans},$$

where

BrstPress = Burst Pressure (psig)

FM1 = Percentage of Failure Mode 1 (Matrix Cracking)

Temp = Temperature (°F)

PresSch = Pressurization Scheme Categorical Variable

Trans = Transducer Location Categorical Variable.

In order to determine the effects of the two defective bottles on the statistical analysis, the 15-17 and the 8-8 bottles were removed from the testing group. Using the same failure mode ranges, a burst pressure equation was generated. The worst case error of the burst pressure equation improved from -14% to +10%, while the multiple correlation coefficient increased from 65% to 75.8%. The regression analysis used both the failure modes for matrix cracking and delaminations to generate the following equation:

$$\text{BrstPress} = -9953 + 12967 \text{ FM1} + 13824 \text{ FM2} - 1.13 \text{ Temp} - 83 \text{ Trans}$$

where

BrstPress = Burst Pressure (psig)

FM1 = Percentage of Failure Mode 1 (Matrix Cracking)

FM2 = Percentage of Failure Mode 2 (Delaminations)

Temp = Temperature (°F)

Trans = Transducer Location Categorical Variable.

The percent error of this burst pressure equation was slightly better than that of the equation generated using the defective bottles. However, the 10% error was still slightly higher than the target value of $\pm 5\%$ and much higher than the $\pm 1.0\%$ values obtained by Kalloo with his hand-tailored analysis.

5.2 NEURAL NETWORK RESULTS

The procedure used for this part of the research was similar to the research performed by Hill, Walker, and Rowell (Section 4.2). An artificial neural network was

used to form a burst pressure prediction model using AE amplitude distribution data as the inputs. The network was formed using the NEURALWORKS PROFESSIONAL II/PLUS software by NeuralWare. During this portion of the research, a set of pressure vessels were used to “train” the network, while the remaining bottles were used as a test set. The actual burst pressures were supplied as target values for the supervised training phase.

Architecturally, the optimized feedforward backpropagation neural network consisted of either a 41 or 42 neuron input layer, a single hidden layer, and an output layer. In the case of the 42 neuron input layer, the inputs were integer variables representing the event frequencies at each amplitude from 60 to 100 dB that occurred during the acoustic emission test plus a categorical variable for burst temperature. The categorical variable allowed the network to easily recognize the difference in the various temperatures. The 41 neuron input layer network was used to determine how well the neural network would predict on the bottles if it was not given the categorical variable for temperature.

The number of hidden layers was optimized to a single hidden layer, although networks with multiple hidden layers were also tested. The optimum number of nodes in the hidden layer was determined through experimentation and varied between 15 and 22 for each test. The number of nodes in this layer is crucial to the output of the network. If too many nodes are employed, the network will fit the training data very closely but will not predict well on the test data. Conversely, if too few nodes are used, the network will fit neither the training nor the test data well. The number of nodes used was considered optimum when the errors for the training set were of the same magnitude of those from the test set.

The output vector was a single variable that represented the predicted burst

pressure for the bottle. During the training phase, the target output for the network was the actual burst pressure. The architecture of the network can be seen in Figure 5.2.

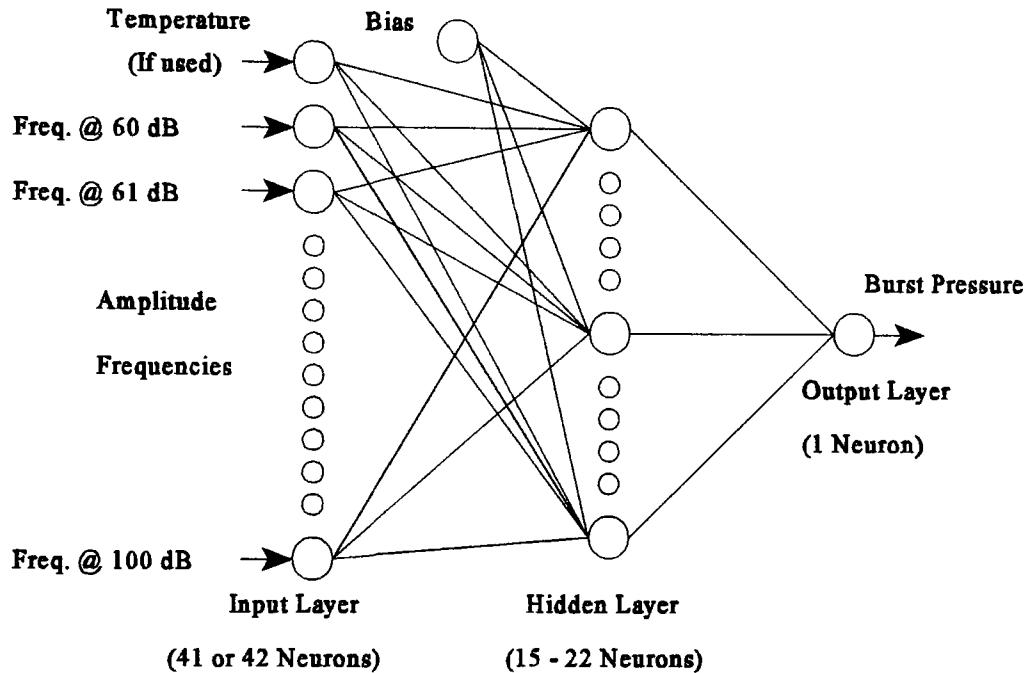


Figure 5.2 Neural Network for Burst Pressure Prediction

The parameters used in the NEURALWORKS PROFESSIONAL II/PLUS software package were kept the same for each of the networks generated for this research. Bias neurons were used to keep the hyperbolic tangent transfer function operating at midrange values where learning is the fastest [11]. The optimal learning coefficient and momentum for this research were determined to be 0.005 and 0.5 respectively. The learning rule employed was the normalized cumulative delta, and the error was calculated over the entire training set (epoch = 6-8). The learning coefficient was multiplied by a factor of 0.5 after every 2500 cycles. A convergence criterion of 0.15 was used to keep the network from memorizing the training data set. Table 5.5

provides a summary of all the neural network parameters.

Table 5.5 Neural Network Parameters

Input Layer	41 or 42
Middle Layer	15 22
Output Layer	1
Bias	Yes
Learning Coefficient	0.005
Momentum	0.5
Learning Rule	Norm. Cum. Delta
Transfer Function	Hyperbolic Tangent
Convergence Threshold	0.15

The failure mechanisms, as represented by the AE amplitude distribution, and the temperature were assumed to be the primary independent variables for this research. Because they were not found to be statistically significant, it was assumed that the network would not need categorical variables for either the two different pressurization schemes or the two transducer configurations. If the network did not train effectively, then a variable for pressurization scheme or transducer configuration could be added at a later time.

Five of the eleven bottles were tested at room temperature (70°F), three were tested at freezing (32°F), and three were tested at 110°F. The neural network was trained on a total of seven bottles, while the remaining four bottles were used as a test set to evaluate the accuracy of the network in making burst pressure predictions.

The first network trained used one of the manufactured defective bottles in the

training set, and the other was used in the test set. The number of hidden layer nodes was optimized to 18, yielding a worse case error of +15.2%. This can be seen in Table 5.6. This rather large error was obtained on the tested manufactured defective bottle, while the other tested bottles had very low errors (the largest being -3.1 %).

Table 5.6 Results of Neural Network using Temperature
(1 Defect in Train; 1 Defect in Test)

	Bottle Serial Number	Temperature at Burst (°F)	Predicted Burst Pressure (psi)	Actual Burst Pressure (psi)	Percent Difference (%)
Training Set	15-17 Def.	70	2329	2257	+ 3.2
	22-24	70	2605	2636	- 1.2
	27-28	70	2812	2816	- 0.2
	33-35	32	2776	2730	+ 1.7
	39-45	32	2891	2959	- 2.3
	78-112	110	2753	2754	- 0.1
	165-187	110	2813	2789	+ 0.9
Testing Set	8-8 Def.	70	2814	2444	+ 15.2
	18-20	70	2687	2773	- 3.1
	57-66	32	2866	2887	- 0.7
	72-77	110	2817	2833	- 0.6

The large prediction error on the defective bottle and the small errors on the nondefective bottles indicated that the network was not recognizing the differences between the two from the data given. Therefore, the two defective bottles were switched such that the 8-8 bottle was now in the training set, and the 15-17 bottle was in the test set. This was done to determine if only one of the bottles was an outlier. This network was optimized by a 15 node hidden layer. Table 5.7 summarizes the training and test

results from this network.

Table 5.7 Results of Neural Network using Temperature
(1 Defect in Train; 1 Defect in Test)

	Bottle Serial Number	Temperature at Burst (°F)	Predicted Burst Pressure (psi)	Actual Burst Pressure (psi)	Percent Difference(%)
Training Set	8-8 Def.	70	2490	2444	+ 1.9
	22-24	70	2669	2636	+ 1.3
	27-28	70	2817	2816	0.0
	33-35	32	2708	2730	- 0.8
	39-45	32	2899	2959	- 2.0
	78-112	110	2762	2754	+ 0.2
	165-187	110	2802	2789	+ 0.5
Testing Set	15-17 Def.	70	2588	2257	+ 14.7
	18-20	70	2700	2773	- 2.6
	57-66	32	2896	2887	+ 0.3
	72-77	110	2827	2833	- 0.2

Again the defective bottle gave the largest error (+14.7 %) with the other test bottles having relatively small errors. This demonstrated that the network was again not distinguishing between the defective and nondefective bottles. While, in reality, the simulated defects lowered the overall burst pressures of the two bottles significantly -- both being a great deal (400 - 700 psig) lower than the nondefective bottles tested -- the neural network treated these two bottles as if they had no defects and predicted nonconservatively, i.e., both burst pressure predictions on the defective bottles were a great deal higher than their actual burst pressures.

Both of the defective bottles were put into the training set for the third network.

It was hoped that this would allow the network to predict on these two bottles with greater accuracy. The results of this network are given in Table 5.8.

Table 5.8 Results of Neural Network using Temperature
(Both Defective in Training Set)

	Bottle Serial Number	Temperature at Burst (°F)	Predicted Burst Pressure (psi)	Actual Burst Pressure (psi)	Percent Difference(%)
Training Set	15-17 Def	70	2336	2257	+ 4.3
	8-8 Def	70	2549	2444	+ 3.5
	22-24	70	2592	2636	- 1.7
	27-28	70	2742	2816	- 2.6
	33-35	32	2801	2730	+ 2.6
	39-45	32	2836	2959	- 4.2
	78-112	110	2756	2754	+ 0.1
	165-187	110	2796	2789	+ 0.3
Testing Set	18-20	70	2556	2773	- 7.8
	57-66	32	2784	2887	3.6
	72-77	110	2772	2833	- 2.1

This network did predict to a greater accuracy on the defective bottles and also lowered the worst case prediction error to -7.8%, which was fairly close to the target range of $\pm 5.0\%$. The three predicted burst pressures for the test bottles were all below the actual burst pressures and were therefore conservative. This is probably due to the defective bottles biasing the network so that the prediction model would generate burst pressures that are lower than the actual pressures.

Hill, Walker, and Rowell [1] did not have defective bottles in their graphite/epoxy bottles and generated a prediction model to -3.89%. In order to determine whether or not

the network could predict as accurately on the undefective fiberglass/epoxy bottles, the two defective bottles were removed from the training group. The network was then optimized to a 22 node hidden layer. Table 5.9 summarized the results of this network.

Table 5.9 Results of Neural Network using Temperature
(NO Defective Bottles)

	Bottle Serial Number	Temperature at Burst (°F)	Predicted Burst Pressure (psi)	Actual Burst Pressure (psi)	Percent Difference(%)
Training Set	22-24	70	2654	2636	+ 0.7
	27-28	70	2822	2816	+ 0.2
	33-35	32	2778	2730	+ 1.8
	39-45	32	2896	2959	- 2.1
	78-112	110	2763	2754	+ 0.3
	165-187	110	2799	2789	+ 0.4
Testing Set	18-20	70	2751	2773	- 0.8
	57-66	32	2893	2887	+ 0.2
	72-77	110	2819	2833	- 0.5

The network trained and tested extremely well when not using the defective bottles with a highest error in the testing of only -0.8% and a highest percent error of -2.1% for all the bottles. Each of these errors is well within the desired goal of $\pm 5\%$.

The final trained network eliminated the categorical variable for temperature in order to determine if the neural network could automatically determine the effect of temperature on the AE data and on the burst pressures. This network was optimized by a 19 node hidden layer. The training and testing sets were the same as for the previous network (without using the defective bottles), so that a comparison of the errors for the

two networks could be made. The results of the previous network and the non-temperature network are presented in Table 5.10.

Table 5.10 Results of Network With and Without Temperature
(NO Defective Bottles)

	Bottle Serial Number	Temperature at Burst (°F)	Actual Burst Pressure (psi)	Percent Difference w/ Temperature (%)	Percent Difference w/out Temperature (%)
Training Set	22-24	70	2636	+ 0.7	+ 0.2
	27-28	70	2816	+ 0.2	+ 0.4
	33-35	32	2730	+ 1.8	+ 0.6
	39-45	32	2959	- 2.1	- 2.8
	78-112	110	2754	+ 0.3	+ 0.4
	165-187	110	2789	+ 0.4	+ 1.9
Testing Set	18-20	70	2773	- 0.8	- 1.5
	57-66	32	2887	+ 0.2	- 0.1
	72-77	110	2833	- 0.5	+ 1.0

Although the percent differences were slightly higher when the categorical variable for temperature was not used, the results show that the network was able to automatically determine the effects of temperature on the AE data and on the burst pressures. The largest percent error was -2.8% on the bottle that had the highest burst pressure of the group.

5.3 SUMMARY OF RESULTS

In summary, for the multivariate statistical analysis performed herein, fixed failure mechanism bands were applied to the amplitude distributions for all eleven fiberglass/epoxy bottles. The optimum failure mechanism bands resulted in a prediction equation that had a worst case prediction error of -14% and a correlation coefficient of 49.9%. When the defective bottles were left out of the analysis, the results improved to a +10% worst case error and a 65.0% correlation coefficient. Kalloo [2], on the other hand individually fit curves to each of the three failure mechanism humps; as such, there was considerable variation in the amplitude bands from bottle to bottle. His results, while not directly comparable, since he did not calculate the predication interval, were considerably better.

The neural network results including the defective bottles had the same order of magnitude worst case errors. When one of the defective bottles was included in the training set and the other in the test set, the errors were +15.2% and +14.7%, depending upon which bottle was used for training and which for testing. When the two defective bottles were included in the training set, the worst case prediction error decreased to -7.8%. Removing the two defective bottles from consideration and performing the neural network analysis on the remaining nine bottles led to a worst case testing errors of -0.8% and -1.5%, the former result being with temperature included as an independent variable and the latter without; the corresponding training errors were -2.1% and -2.8%, respectively. In this case, the training errors were slightly larger than the testing errors (but not significantly different). Thus, the neural networks predicted extremely well on the nondefective bottles and rather poorly on the defective bottles. However, it did appear that the more defective bottles used in the training set, the better the results.

6.0 CONCLUSIONS AND RECOMMENDATIONS

6.1 CONCLUSIONS

The following conclusions can be made from the results of the statistical analysis performed herein:

1. Statistical analysis using fixed failure mechanism bands from the amplitude distributions was not able to generate a burst pressure prediction equation with the desired $\pm 5\%$ worst case error.
2. Fixed amplitude intervals probably cannot accommodate the normal variations in attenuation that occur between bottles because of transducer placement and therefore result in improper modeling of the failure mechanism bands.
3. The low correlation coefficients for the burst pressure prediction equations indicated that either the amplitude ranges were not properly modeling the failure mechanisms in fiberglass/epoxy or failure mechanism information is not readily discernible from the amplitude distributions.

The results of the artificial neural network analysis lead to the following conclusions:

1. Using the amplitude distribution data as input, a neural network was able to predict burst pressures extremely well in the nondefective bottles -- even without using temperature as an independent variable -- the largest percent error of -2.8% being well within the goal of $\pm 5\%$.
2. The neural networks were not able to distinguish the defective bottles on such a small test set (two defective bottles out of eleven). More defective bottles would be necessary to increase the prediction accuracy.
3. The neural networks were able to determine the effects of pressurization scheme, transducer configuration, and temperature from the amplitude distributions themselves without having to explicitly input any of these variables.

The following general conclusions can be made from the research presented herein:

1. An artificial neural network could be used to accurately determine the burst pressures of filament wound composite pressure vessels while using the data taken at proof testing loads of 25% of the expected burst pressure. This has been proven in previous research by Hill, Walker, and Rowell [1] on a series of graphite/epoxy bottles and the research presented here on a series of fiberglass/epoxy bottles.

2. The neural networks predicted burst pressures to a greater accuracy than multivariate statistical analysis. This could be explained by the fact that the statistical analysis generates a linear burst pressure equation, whereas the neural network is not limited to linear modeling.
3. Amplitude distributions may not provide adequate discrimination for burst pressure prediction in defective bottles. Additional AE parameters, such as energy or duration may be needed to obtain better results for defective bottles.
4. The use of multivariate statistics required a great deal more intuition as to which variables were important in the regression analysis than the use of a neural network, which automatically determined what was important and what was not.

6.2 RECOMMENDATIONS

The multivariate statistical analysis results could be improved by using a Kohonen self organizing map (SOM) neural network to automatically sort the AE data into failure mechanism clusters. This would eliminate the need for Gaussian and Rayleigh distributions and the human error associated with determining the appropriate AE amplitude ranges. A burst pressure prediction equation could then be generated, as before, from the percentages of events in the various clusters.

If a larger sample of defective bottles had been tested, an artificial neural network should have been able to identify the defective bottles and predict on the burst pressures more accurately. Defective bottles tested at temperatures other than 70°F would also be very beneficial in determining whether this hypothesis is correct. Finally, the use of an

additional AE parameter (such as energy or duration) as input to the neural network may provide the information necessary to accurately predict burst pressures in defective pressure vessels.

7.0 REFERENCES

1. Hill, Eric v. K., James L. Walker II, and Ginger H. Rowell, "Burst Pressure Prediction in Graphite/Epoxy Pressure Vessels using Neural Networks and Acoustic Emission Amplitude Data," *Materials Evaluation*, Vol. 54, No. 6, 1996, pp. 744-748, 754.
2. Kalloo, Frederick R., "Predicting Burst Pressures in Filament Wound Composite Vessels Using Acoustic Emission Data," M.S. Thesis, Embry-Riddle Aeronautical University, 1988.
3. Walker, James L., "Composite Structure Ultimate Strength Prediction from Acoustic Emission Amplitude Data," M.S. Thesis, Embry-Riddle Aeronautical University, 1990.
4. Walker, James L., and Eric v. K. Hill, "Composite Ultimate Strength Prediction from Acoustic Emission Amplitude Data," presented at the 3rd Conference on Nondestructive Evaluation for Aerospace Requirements, Huntsville, AL, June 4-6, 1991.
5. Hill, Eric v. K. and Ted J. Lewis, "Acoustic Emission Burst Pressure Prediction in 14.6 cm (5.75 inch) Diameter Fiberglass/Epoxy Pressure Vessels", Proceedings of 35th International SAMPE Symposium and Exhibition, Society for the Advancement of Materials and Process Engineering, Covina, Ca., 1990, pp. 2189-2201.
6. Tenant-Smith, J., Basic Statistics, Butterworth & Co. Ltd., London, UK, 1985, p. 106.
7. Kouvarakos, M., and Eric v. K. Hill, "Isolating Tensile Failure Mechanisms in Fiberglass/Epoxy from Acoustic Emission Signal Parameters," *Materials Evaluation*, Vol. 53, No. 3, 1995.
8. Hubele, N.F., and H.B. Hwarng, "A Neural Network Model and Multiple Linear Regression" in C.H. Dagli, B.R. Fernandez, J. Ghosh, and R.T.S. Kumara, eds., Intelligent Engineering Systems Through Artificial Neural Networks, Vol. 4, American Society of Mechanical Engineering Press, New York, NY, 1994, pp. 199-203.

- 9 Fausett, L V , Fundamentals of Neural Networks Architectures, Algorithms, and Applications, Prentice Hall, Englewood Cliffs, NJ, 1994, pp 328-330
- 10 Hill, Eric v K , “Predicting Burst Pressures in Filament-Wound Composite Pressure Vessels by Using Acoustic Emission Data,” *Materials Evaluation*, December 1992, p 1439-1445
- 11 Hill, Eric v K , “Neural Network Prediction of Aluminum-Lithium Weld Strengths from Acoustic Emission Amplitude Data,” *Materials Evaluation*, 1993, p 1040-1051

APPENDICES

APPENDIX A

AMPLITUDE DISTRIBUTIONS

4 Ch, A-Dump is OFF

NON-CUMULATIVE

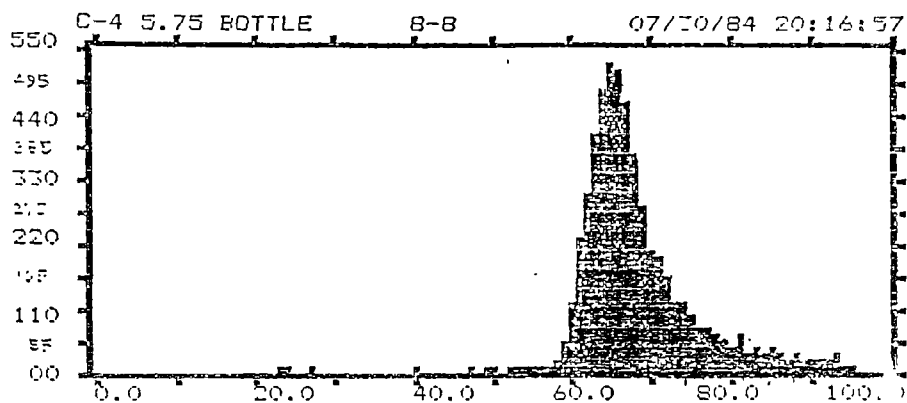
INTERVAL SUM

EVENTS

FIRST ARRIVAL

EVENTS = 5720

GRAPH 1 OF 5



Scroll for menu

NON-CUMULATIVE AMPLITUDE FIRST ARRIVAL

4 Ch, A-Dump is OFF

NON-CUMULATIVE

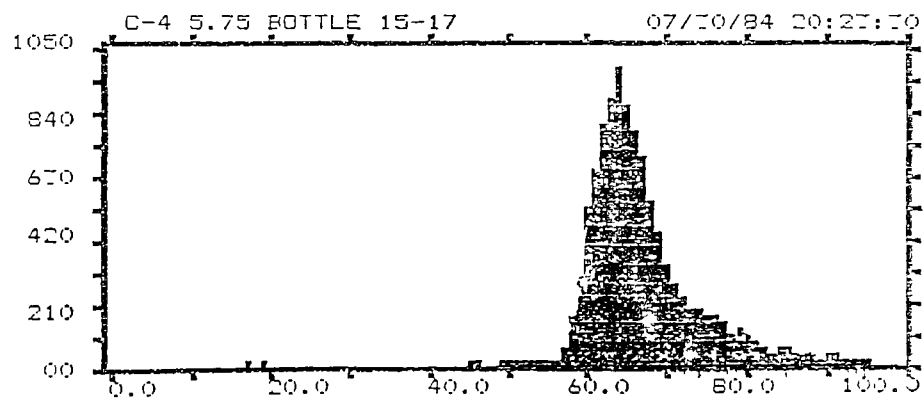
INTERVAL SUM

EVENTS

FIRST ARRIVAL

EVENTS = 10701

GRAPH 1 OF 5



Scroll for menu

NON-CUMULATIVE AMPLITUDE FIRST ARRIVAL

4 Ch, A-Dump is OFF

NON-CUMULATIVE

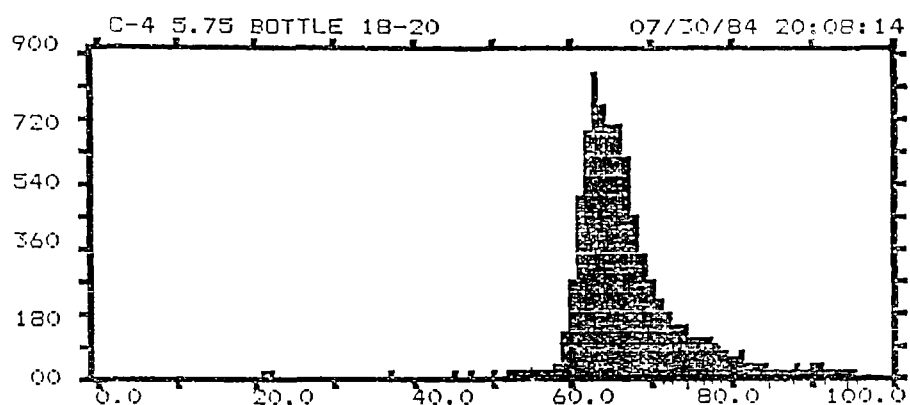
INTERVAL SUM

EVENTS

FIRST ARRIVAL

EVENTS = 8315

GRAPH 1 OF 5



Scroll for menu

NON-CUMULATIVE AMPLITUDE FIRST ARRIVAL

4 Ch, A-Dump is OFF

NON-CUMULATIVE

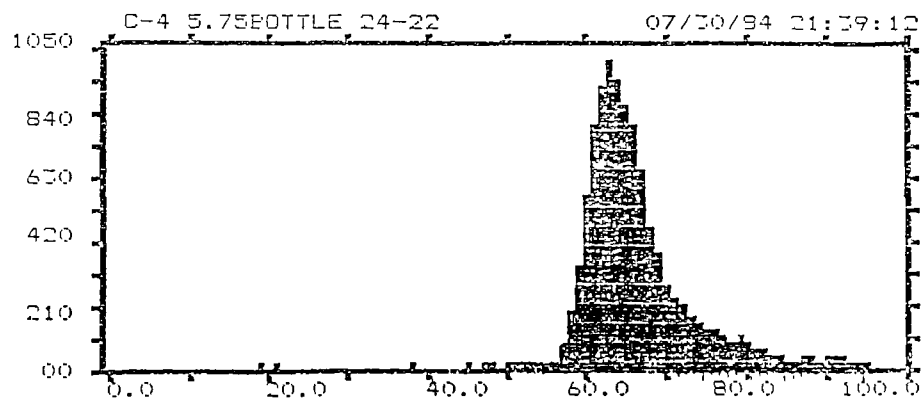
INTERVAL SUM

EVENTS

FIRST ARRIVAL

EVENTS = 10692

GRAPH 1 OF 5



Scroll for menu

NON-CUMULATIVE AMPLITUDE FIRST ARRIVAL

4 Ch, A-Dump is OFF

NON-CUMULATIVE

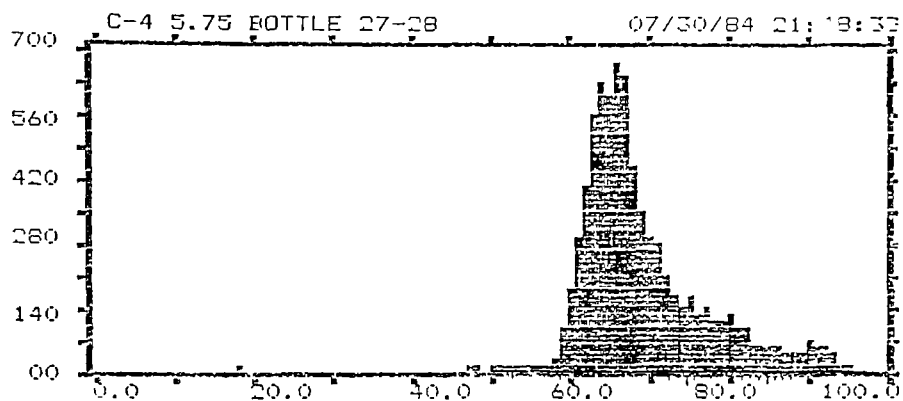
INTERVAL SUM

EVENTS

FIRST ARRIVAL

EVENTS = 7829

GRAPH 1 OF 5



Scroll for menu

NON-CUMULATIVE AMPLITUDE FIRST ARRIVAL

4 Ch, A-Dump is OFF

NON-CUMULATIVE

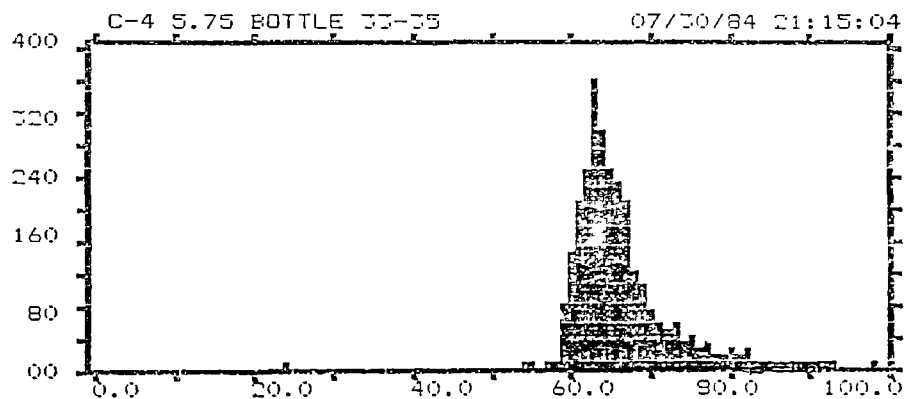
INTERVAL SUM

EVENTS

FIRST ARRIVAL

EVENTS = 2886

GRAPH 1 OF 5



Scroll for menu

NON-CUMULATIVE AMPLITUDE FIRST ARRIVAL

4 Ch, A-Dump is OFF

NON-CUMULATIVE

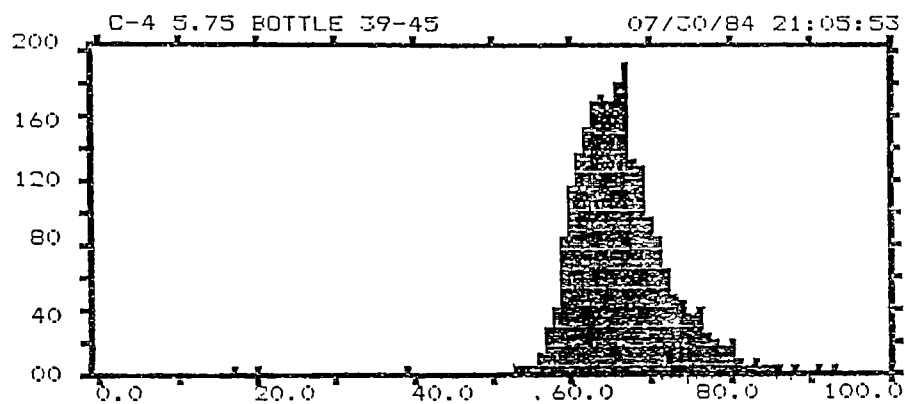
INTERVAL SUM

EVENTS

FIRST ARRIVAL

EVENTS = 2299

GRAPH 1 OF 5



Scroll for menu

NON-CUMULATIVE AMPLITUDE FIRST ARRIVAL

4 Ch, A-Dump is OFF

NON-CUMULATIVE

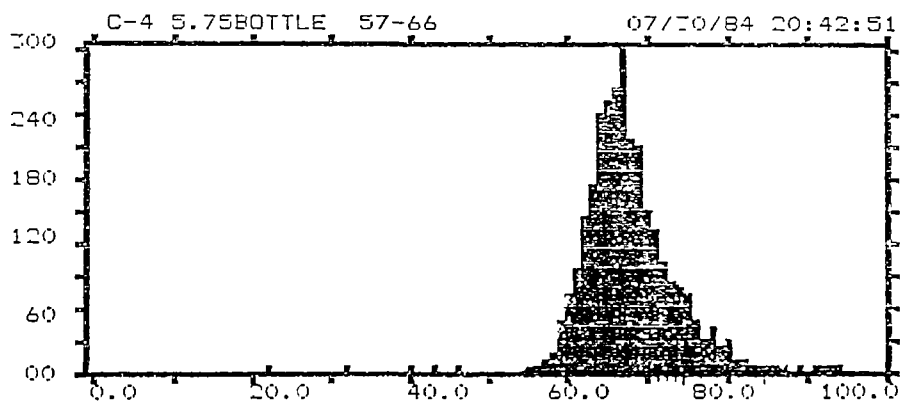
INTERVAL SUM

EVENTS

FIRST ARRIVAL

EVENTS = 2966

GRAPH 1 OF 1



Scroll for menu

NON-CUMULATIVE AMPLITUDE FIRST ARRIVAL

4 Ch, A-Dump is OFF

NON-CUMULATIVE

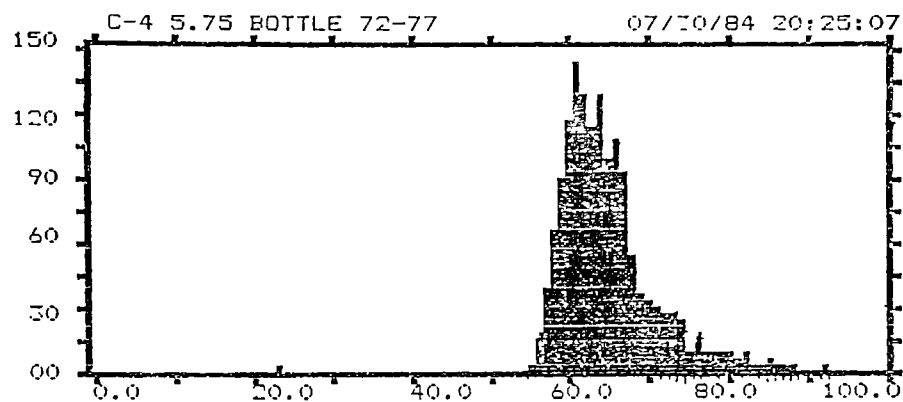
INTERVAL SUM

EVENTS

FIRST ARRIVAL

EVENTS = 1507

GRAPH 1 OF 5



Scroll for menu

NON-CUMULATIVE AMPLITUDE FIRST ARRIVAL

4 Ch, A-Dump is OFF

NON-CUMULATIVE

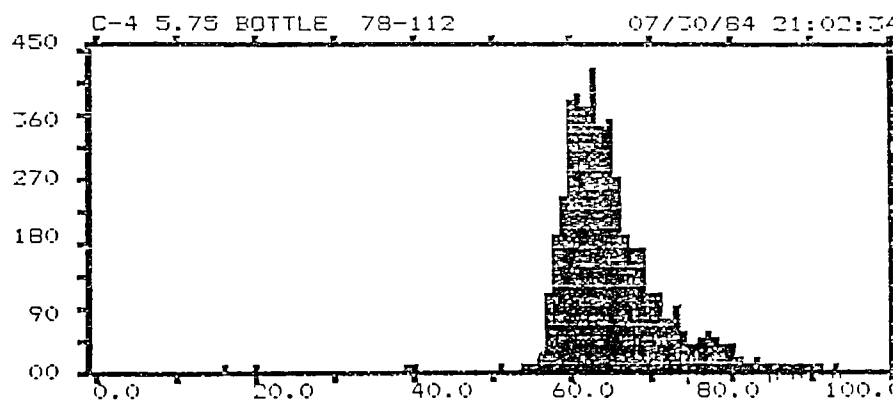
INTERVAL SUM

EVENTS

FIRST ARRIVAL

EVENTS = 4542

GRAPH 1 OF 5



Scroll for menu

NON-CUMULATIVE AMPLITUDE FIRST ARRIVAL

4 Ch, A-Dump is OFF

NON-CUMULATIVE

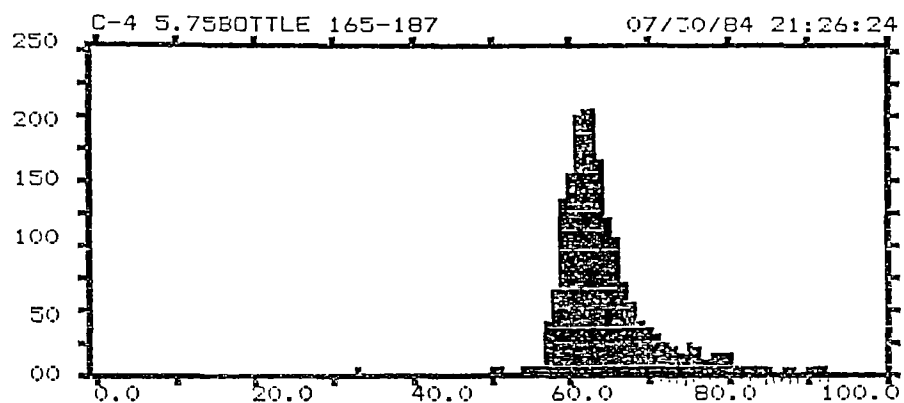
INTERVAL SUM

EVENTS

FIRST ARRIVAL

EVENTS = 1882

GRAPH 1 OF 5



Scroll for menu

NON-CUMULATIVE AMPLITUDE FIRST ARRIVAL

APPENDIX B

MINITAB REGRESSION ANALYSIS

MTB > Regress 'BrstPres' 4 'H1' 'Temp' 'PresSch' 'Trans'.

The regression equation is

BrstPres = - 6066 + 9836 H1 - 1.74 Temp + 1046 PresSch - 952 Trans

Predictor	Coef	Stdev	t-ratio	p
Constant	-6066	3480	-1.74	0.132
H1	9836	3822	2.57	0.042
Temp	-1.737	1.305	-1.33	0.232
PresSch	1046.2	430.7	2.43	0.051
Trans	-952.4	291.0	-3.27	0.017

s = 120.3 R-sq = 79.0% R-sq(adj) = 65.0%

Analysis of Variance

SOURCE	DF	SS	MS	F	p
Regression	4	326385	81596	5.64	0.031
Error	6	86877	14479		
Total	10	413262			

SOURCE	DF	SEQ SS
H1	1	64925
Temp	1	9640
PresSch	1	96704
Trans	1	155116

Unusual Observations

Obs.	H1	BrstPres	Fit	Stdev.Fit	Residual	St.Resid
1	0.870	2257.0	2463.6	65.1	-206.6	-2.04R
5	0.809	2816.0	2816.0	120.3	0.0	* X

.R denotes an obs. with a large st. resid.

X denotes an obs. whose X value gives it large influence.

MTB > Regress 'BrstPres' 5 'H1' 'H2' 'Trans' 'PresSch' 'Temp'.

* PresSch is highly correlated with other X variables
 * PresSch has been removed from the equation

The regression equation is

BrstPres = - 9953 + 12967 H1 + 13824 H2 + 83.0 Trans - 1.13 Temp

Predictor	Coef	Stdev	t-ratio	p
Constant	-9953	3571	-2.79	0.069
H1	12967	3708	3.50	0.040
H2	13824	4827	2.86	0.064
Trans	82.98	94.97	0.87	0.447
Temp	-1.1322	0.6021	-1.88	0.157

s = 48.67 R-sq = 89.6% R-sq(adj) = 75.8%

Analysis of Variance

SOURCE	DF	SS	MS	F	p
Regression	4	61406	15351	6.48	0.078
Error	3	7105	2368		
Total	7	68511			

SOURCE	DF	SEQ SS
H1	1	25352
H2	1	27665
Trans	1	12
Temp	1	8376